**RESEARCH ARTICLE**

# Oxidative Leaching of Akpugo Kaolinite for Alumina Recovery and Kinetic Modeling
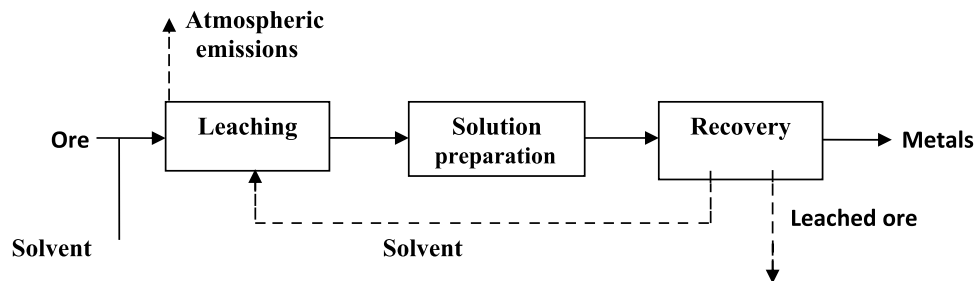
Ikechukwu A. Nnanwube[1] · Okechukwu D. Onukwuli[2]

## Abstract

In this work, the kinetics of alumina recovery from Akpugo kaolinite in nitric acid and hydrogen peroxide binary solution are investigated. Parameters considered in the study include the leaching temperature, hydrogen peroxide concentration, stirring rate, solid/liquid (S/L) ratio, and particle size. The fraction of alumina dissolved increases with increase in leaching temperature, hydrogen peroxide concentration, and stirring rate, from 47.6 to 87.3% for temperatures of 30 and 90 °C; 48 to 85.6% for concentrations of 2 and 10 M; and 49.8 to 86.8% for stirring rates of 90 and 540 rpm. The fraction of alumina dissolved, however, decreases with increase in S/L ratio and particle size, from 86.6 to 50.2% for solid/liquid ratios of 20 and 45 g/L and 87.6 to 49.3% for particle sizes of < 75 and < 425 μm. The experimental data fitted into the product layer diffusion model while surface chemical reaction was the rate-determining step. Activation energy was estimated to be 26.56 kJ/mol while the Arrhenius constant of 25.01 s$^{-1}$ was estimated. About 87.1% alumina dissolution rate was recorded at the optimum conditions. The overall reaction constant was estimated to be 8.883 s$^{-1}$. Post-leaching analysis of the leached residue by XRD revealed the presence of illite and quartz.

## Graphical Abstract

The contributing editor for this article was Grace Ofori-Sarpong.

✉ Ikechukwu A. Nnanwube
  ik.nnanwube@gmail.com

1 Department of Chemical Engineering, Madonna University, Akpugo, Nigeria

2 Department of Chemical Engineering, Nnamdi Azikiwe University, Awka, Nigeria

## Introduction

Clay minerals belong to the universal but significant set within the phyllosilicates that contain large percentages of water amid their silicate sheets. The majorities of the clays are chemically and structurally similar to other phyllosilicates but contain varying quantities of water and permit additional replacement of their cations. There are numerous significant applications and considerations of clay minerals. They are applied in paper production, drilling, construction, and manufacturing. Clay minerals are made up of mostly

silica, alumina, and water, though they may also have substantial amounts of iron, alkaline, and alkaline earths. Clay is produced through chemical and mechanical breakdown of rocks. There are six categories of clay according to the U. S. Bureau of Mines. The categories are bentonite, fire clay, fuller's earth, kaolin, ball clay, as well as common clay and shale [1, 2].

Kaolin, also known as China clay is defined as a white clay-like material made up of mostly kaolinite which is a hydrated aluminum silicate ($Al_2O_3 \cdot 2SiO_2 \cdot 2H_2O$), and other kaolin-group minerals. The major impurities in kaolinite clay are biotite, ilmenite, limonite, siderite, and other carbonaceous materials. Kaolin has a broad range of industrial uses which include fiberglass and insulation, paint, rubber, ceramics, refractories, paper coating and filling, and chemicals. Ball clay is a plastic, white-firing clay which is made up of principally kaolinite and is deployed mostly for dinnerware, bonding in ceramic ware, pottery, floor and wall tile, and sanitary ware. Fire clays are made up of principally kaolinite but may also contain a number of other materials which include burley flint, diaspore, burley, ball clay, bauxitic clay, and shale. Due to their capability to endure temperatures of 1500 °C (2700 °F) or higher, fire clays are commonly applied in refractories or to increase vitrification temperatures in weighty clay products [1, 2].

Alumina, which constitutes over 25% of kaolin, is broadly applied as a superior material as a result of its blend of chemical, physical, and electrical properties. Due to its hardness and strength with excellent wear and chemical resistance at increased temperatures, it has become a material of choice for significant structural applications. Alumina has also found major application in the electrical and electronic sectors due to its exceptional dielectric and insulating properties. Other areas where alumina is applied include high-grade polishes, fireproof plastics, biofuel and cell fuel, and refractories. Alumina of high purity deployed for high technical applications is needed to have over 95% purity with very little sodium and iron content [1, 2].

Currently, bauxite is the major raw material from which alumina is produced in most parts of the world through the Bayern process [3]. Bauxite is a weathered rock having two types of hydrated aluminum oxide, which could be mainly a monohydrate (AlO(OH)) in caustic bauxite or mainly a trihydrate ($Al(OH)_3$) in laterite bauxite. However, the production of bauxite is concentrated in very few countries having abundant deposits of bauxite ore. Moreover, the Bayer process has been reported to be associated with the generation of abundant quantities of alkaline-rich bauxites residues, making the process potentially hazardous to the immediate environment [4–7]. This necessitates its substitution with other readily available raw material such as kaolinite, especially in countries with little or no bauxite deposits. The feasibility of alumina recovery from kaolinitic clay as a substitute to bauxite has been explored by both acidic and alkaline routes [6–11]. To enhance alumina recovery rate from kaolinitic clay, the clay samples are normally calcined in the temperature range of 500–750 °C before leaching. This helps boost the reactivity of the particles by making the aluminum in the clay matrix more soluble and also helps remove organic material in the pores [8]. Kaolinite is also changed to meta-kaolin from which the aluminum is dissolved as acid salt [8, 9].

Some researchers have developed different procedures for alumina recovery from kaolinite using different leachants [8, 12–15]. In these studies, leachants such as nitric acid, hydrochloric acid, sulfuric acid, oxalic acid, and sodium hydroxide were deployed, with varying degrees of metal recovery. There are very few reported studies – to our knowledge – on the use of hydrogen peroxide as a leachant for alumina recovery from kaolinite and other clay minerals [6, 7] despite its viability for improved metal recovery in leaching operations [16, 17]. However, there is no reported work – to our knowledge – on alumina recovery from Akpugo kaolinite. Hence, the synergistic effect of nitric acid and hydrogen peroxide for alumina recovery from kaolinite obtained from Akpugo in south-eastern Nigeria was explored in this study. Process variables investigated in this study include leachant concentration, temperature, stirring rate, solid/liquid ratio, and particle size, while the shrinking core models were used for the kinetic analysis. This study was, therefore, aimed at reducing alumina processing costs by the use of readily available and cheaper raw material and improving the product purity through enhanced alumina recovery efficiency.
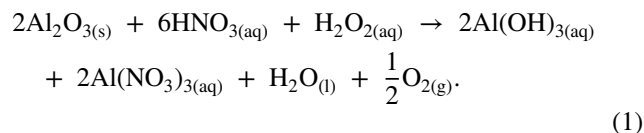
## Materials and Method

### Materials

#### Sourcing and Preparation of Samples

The kaolinite sample deployed for this work was obtained from Akpugo in Nkanu West Local Government Area (L. G. A.) of Enugu State, Nigeria. The clay sample was firstly crushed and reduced to fine particles using a laboratory crusher [10, 15]. The clay sample was dried under the sun for 48 h and then calcined within a temperature range of 500–800 °C for 1 h to enhance alumina recovery. The calcined clay sample was further pulverized and sieved into five different particle sizes: < 75, − 106 + 75, − 212 + 106, − 300 + 212, and < 425 μm, using ASTM standard test sieves [18]. Analytical grades of hydrogen peroxide and nitric acid were used to prepare all solutions with the aid of deionized water. All experiments unless otherwise stated were performed using < 75 μm particle size fraction due to its high surface area.

## Experimental Procedure

Experiments were first carried out with the calcined clay samples to determine the optimum calcinations temperature. The experiments were conducted in a 500 mL glass reactor which was continuously stirred with a magnetically stirred hot plate [14, 19–21]. For each run, 100 mL of a binary solution of nitric acid ($HNO_3$) and hydrogen peroxide ($H_2O_2$) at different concentrations (2–12 M) were introduced into the flask and temperature was set to the desired value [22, 23]. A 20 g/L of the clay sample was added to the reactor, while the solution was stirred continuously within a time range of (20–150 min). The experiments were duplicated and the average values were reported. Other variables studied include leaching temperature (30–90 °C), solid/liquid ratio (20–45 g/L), and particle size (75–425 μm). The fraction of alumina dissolved in the leach solution was determined using Atomic Absorption Spectrophotometer (AAS) analysis conducted using Agilent Technologies 240FS AA model.

Kinetic plots were carried out to determine the order of reaction and activation energy for better understanding of the dissolution mechanism for the process. The residual product at optimal leaching was characterized using scanning electron microscope (SEM) and X-ray diffraction (XRD) [24–26]. The leaching process is represented by the stoichiometry as follows (Eq. 1):

$$2Al_2O_{3(s)} + 6HNO_{3(aq)} + H_2O_{2(aq)} \rightarrow 2Al(OH)_{3(aq)}$$
$$+ 2Al(NO_3)_{3(aq)} + H_2O_{(l)} + \frac{1}{2}O_{2(g)}. \tag{1}$$

### Scanning Electron Microscope (SEM) Description

About 5 g of each sample was placed on a double adhesive which was on a sample stub. It was coated with 5 nm gold with a sputter coater Q150R ES by quorum. It was then placed in a SEM machine column where it was focused with little brightness and contrast. Thereafter, it was transferred to SEM mode and was stored via USB stick.

### FTIR Analysis Description

The Fourier Transform Infrared (FTIR) (Buck Scientific M350) spectrophotometer was used to determine the functional groups found in the clay. The FTIR spectrum reveals that CH/OH out-of-plane deformation and C–Cl/C–S stretches define the band at 678.4 cm$^{-1}$. The band 779.0 cm$^{-1}$ is credited to $NH_2$ wag and Si–C stretch. The $CH_2$ out-of-plane wag define the very strong band at 909.5 cm$^{-1}$, while the =CH out-of-plane deformation

and P–O–C anti-symmetrical stretch define the band at 995.2 cm$^{-1}$. The C–N/C–O/C=S/C–O–C stretches, C–O–C anti-symmetrical stretch, and C–C–N bending define the band at 1114.5 cm$^{-1}$, while the OH stretch for dilute solution defines the strong bands at 3652.8 cm$^{-1}$ and 3690.1 cm$^{-1}$ [14, 19, 26–31].

### Description on Effect of Calcinations Temperature on Alumina Leaching

The influence of calcinations temperature on the leaching of alumina from Akpugo kaolinite was examined by leaching samples of the clay calcined at temperatures of 500, 600, 700, 750, and 800 °C, in nitric acid solution within a time range of 0–150 min. Other experimental parameters such as nitric acid concentration, stirring rate, leaching temperature, S/L ratio, and particle diameter were maintained at 6 M, 540 rpm, 80 °C, 20 g/L, and < 75 μm, respectively [6, 7].

### Description on Effect of $H_2O_2$ Concentration in the Presence of 10 M $HNO_3$ on Alumina Leaching

The influence of $H_2O_2$ concentration in the presence of 10 M nitric acid on the percentage of alumina dissolved was studied at various $H_2O_2$ concentrations in the range of 2–12 M over a time range of 0–150 min. Other experimental conditions were kept constant, with a particle size of < 75 μm, S/L ratio of 20 g/L, leaching temperature of 80 °C, stirring speed of 540 rpm, and nitric acid concentration of 10 M [6, 7].

### Description on Effect of Stirring Rate on Alumina Leaching

The influence of stirring rate on the leaching of alumina from Akpugo kaolinite was studied using stirring rates of 90, 180, 360, 450, 540, and 720 rpm over a time range of 0–150 min. Other experimental conditions were kept constant, with particle size of < 75 μm, S/L ratio of 20 g/L, temperature of 80 °C, nitric acid concentration of 10 M, and hydrogen peroxide concentration of 10 M [6, 7].

### Description on Effect of Temperature on Alumina Leaching

The influence of temperature was studied using temperatures of 30, 40, 60, 80, and 90 °C while other parameters were maintained, with nitric acid concentration of 10 M, hydrogen peroxide concentration of 10 M, stirring rate of 540 rpm, S/L ratio of 20 g/L, and particle size of < 75 μm over a time range of 0 to 150 min [6, 7].

## Description on Effect of Solid/Liquid Ratio on Alumina Leaching

The influence of S/L ratio on alumina recovery from Akpugo kaolinite was examined with S/L ratios of 20, 25, 30, 35, and 45 g/L over a leaching time range of 0 to 150 min. Other experimental conditions were maintained constant with nitric acid concentration of 10 M, hydrogen peroxide concentration of 10 M, stirring rate of 540 rpm, reaction temperature of 90 °C, and particle size of < 75 μm [6, 7].

## Description on Effect of Particle Size on Alumina Leaching

The effect of particle size on Akpugo kaolinite dissolution in a binary solution of 10 M $H_2O_2$ and 10 M $HNO_3$ was examined using five different fractions such as < 75, 75–106, 106–212, 212–300, and < 425 μm and leaching time varied from 0 to 150 min. Other parameters such as leaching temperature, stirring rate, and S/L ratio were held constant at 90 °C, 540 rpm, and 20 g/L, respectively [6, 7].

## Results and Discussion

### Characterization of Raw Sample

#### Elemental Analysis by XRF

X-ray fluorescence (XRF) was deployed to determine the chemical composition of the clay used in this study before and after calcinations to determine the changes in the chemical composition of the clay as a result of the calcinations [14, 19]. The XRF analysis was conducted using X-supreme 600 oxford instruments.

The result of the X-ray fluorescence (XRF) analysis of Akpugo kaolinite is shown in Table 1. The result shows $Al_2O_3$, $SiO_3$, and $Fe_2O_3$ as the major oxides found in the clay. The minor oxides detected are MgO, $K_2O$, CaO, $Mn_2O_3$, and $TiO_2$ while oxides such as $Cr_2O_3$, ZnO, and SrO were detected as traces. The result shows that the clay

exists mainly as kaolinite. The clay sample calcined at 600 °C was also analyzed by X-ray fluorescence technique. The results showed that calcinations caused some alterations in the chemical composition of the clay. From the results, percentage of aluminosilicate increased from 78.3% for the raw sample to 80.88% for the calcined sample. The percentage of $Fe_2O_3$, however, decreased from 12.65% to 10.58%. Hence, calcination helped further purify the clay. The result of the XRF analysis of the calcined sample is also shown in Table 1 [7, 14].

### Mineralogical Analysis

The mineralogical analysis of Akpugo kaolinite by X-ray diffraction (XRD) was conducted using ARL X'TRA X-ray diffractometer (Thermoscientific) with the serial number 197492086, with $CuK_{\alpha 1}$ (1.54 Å) radiation, generated at 45 kV and 40 mA [32]. The result confirms that the clay exists mainly as kaolinite. Figure 1 shows the results of the XRD of the clay, showing the mineral phases present in the sample. The XRD pattern provided major peaks at 24.84, 26.64, 12.30, 20.86, and 35.88° $2\theta$, respectively, as shown in Fig. 1. The result reveals the presence of kaolinite ($Al_2Si_2O_5(OH)_4$) and quartz ($SiO_2$). All these agree with the results of the X-ray fluorescence (XRF) from elemental analysis [19]. The X-ray diffraction data of raw Akpugo kaolinite are presented in Table 2.

### Morphological Examination by Scanning Electron Microscope (SEM)

The scanning electron microscope (SEM) of Akpugo kaolinite was conducted using Q250 by FEI model microscope, and the result is depicted in Fig. 2 with magnifications of ×500 and ×1000, respectively [14, 19]. The result shows that the kaolinite particles form agglomerates with rough edges. This agrees with the results of Bendou and Amrani [33]. The clay appears to be poorly crystalline and this may be credited to the presence of impurities. A number of authors have observed that illite and other impurities also reduce

**Table 1** XRF result of raw and calcined Akpugo kaolinite

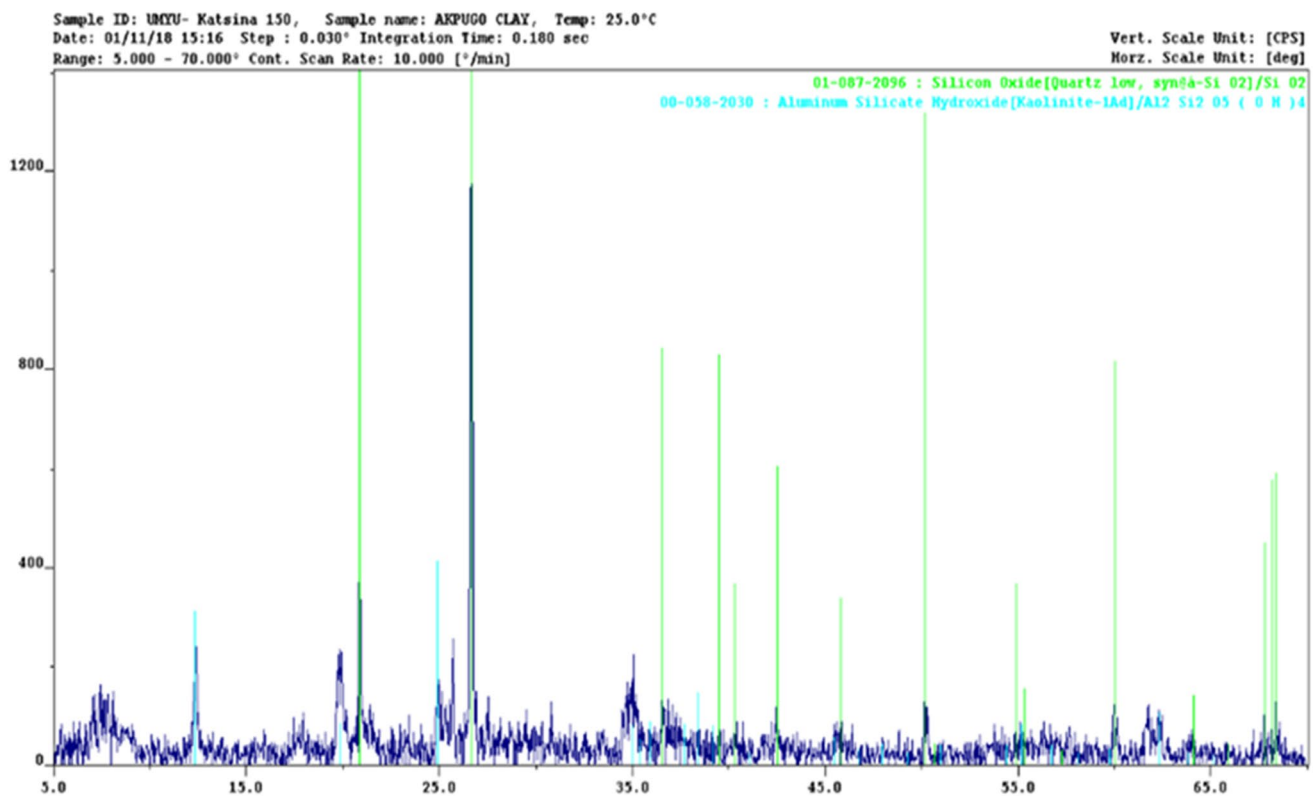| Component | Raw sample (%) | Calcined sample (%) | Component | Raw sample (%) | Calcined sample (%) |
|-----------|----------------|---------------------|-----------|----------------|---------------------|
| $SiO_2$ | 55.64 | 56.56 | MgO | 2.06 | 2.24 |
| $TiO_2$ | 1.91 | 1.59 | CaO | 1.17 | 1.28 |
| $Al_2O_3$ | 22.66 | 24.32 | $K_2O$ | 3.16 | 2.70 |
| $Fe_2O_3$ | 12.65 | 10.58 | SrO | 0.04 | 0.03 |
| $Cr_2O_3$ | 0.03 | 0.02 | $P_2O_5$ | 0.33 | 0.32 |
| ZnO | 0.03 | 0.03 | $SO_3$ | 0.20 | 0.23 |
| MnO | 0.10 | 0.09 | Cl | 0.02 | 0.01 |

**Fig. 1** X-ray diffraction pattern of Akpugo kaolinite

**Table 2** The X-ray diffraction data of Akpugo kaolinite showing the angle $2\theta$ and $d$-values of the compounds identified, with their relative intensity (%)

| $2\theta$ | $d$-Value (Å) | Compound | Intensity (%) | JCPDS file No |
|---|---|---|---|---|
| 12.30 | 7.19 | Kaolinite-1 ($Al_2Si_2O_5(OH)_4$) | 75.28 | 00-058-2030 |
| 19.88 | 4.46 | Kaolinite-1 ($Al_2Si_2O_5(OH)_4$) | 20.62 | 00-058-2030 |
| 20.86 | 4.25 | Quartz ($SiO_2$) | 21.62 | 01-087-2096 |
| 24.84 | 3.58 | Kaolinite-1 ($Al_2Si_2O_5(OH)_4$) | 100.00 | 00-058-2030 |
| 26.64 | 3.34 | Quartz ($SiO_2$) | 100.00 | 01-087-2096 |
| 34.98 | 2.56 | Kaolinite-1 ($Al_2Si_2O_5(OH)_4$) | 19.22 | 00-058-2030 |
| 35.40 | 2.53 | Kaolinite-1 ($Al_2Si_2O_5(OH)_4$) | 13.11 | 00-058-2030 |
| 35.88 | 2.50 | Kaolinite-1 ($Al_2Si_2O_5(OH)_4$) | 21.32 | 00-058-2030 |
| 36.55 | 2.46 | Quartz ($SiO_2$) | 6.01 | 01-087-2096 |
| 39.47 | 2.28 | Quartz ($SiO_2$) | 5.91 | 01-087-2096 |

JCPDS File No.: Joint Committee on Power Diffraction Standards File Number.

the whiteness of kaolinites. Similar results were obtained by previous authors [34–37].

### Results of FTIR Analysis

The FTIR data of raw Akpugo kaolinite are presented in Table 3 while the FTIR spectra are presented in Fig. 3.

### Results on the Effect of Process Parameters

#### Effect of Calcinations Temperature on Alumina Leaching

Alumina recovery rates of 61.7, 72.6, 67.7, 53.7, and 49.8% were achieved after leaching for 150 min with calcination temperatures of 500, 600, 700, 750, and 800 °C, respectively. The results show that maximum dissolution
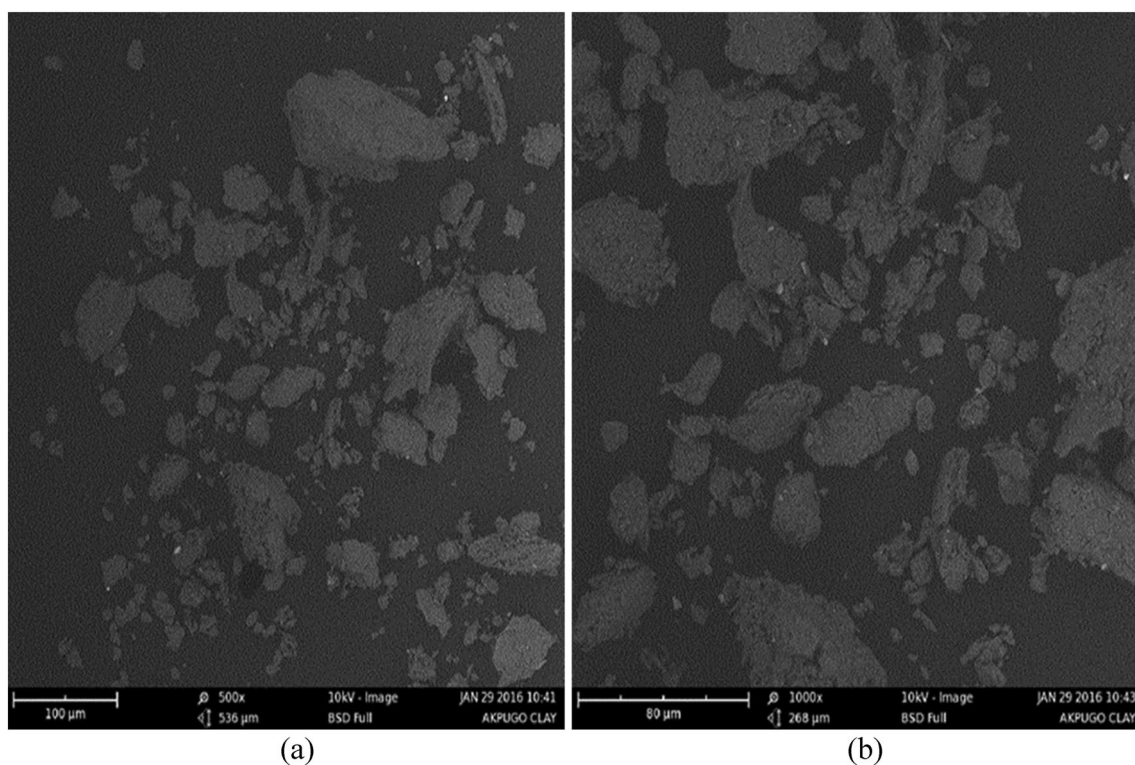
**Fig. 2** SEM images of Akpugo kaolinite showing magnifications of 500× (a) and 1000× (b), respectively

**Table 3** FTIR results of Akpugo kaolinite

| Spectra band (cm$^{-1}$) | Assignment |
| --- | --- |
| 678.4 | CH/OH out-of-plane deformation, C–Cl/C–S stretches |
| 779.0 | NH$_2$ wag/Si–C stretch |
| 909.5 | CH$_2$ out-of-plane wag |
| 995.2 | =CH out-of-plane deformation/ P–O–C anti-symmetrical stretch |
| 1114.5 | C–N/C–O/C=S/C–O–C stretches/ C–O–C anti-symmetrical stretch/C–C–N bending |
| 3652.8 | OH stretch for dilute solution |
| 3690.1 | OH stretch for dilute solution |

rate of 72.6% was attained with calcinations temperature of 600 °C while a minimum dissolution rate of 49.8% was obtained with calcinations temperature of 800 °C in 150 min at the given conditions. Hence, the sample calcined at a temperature of 600 °C was used for subsequent studies. The leaching curves on the effect of calcinations temperature on alumina recovery from Akpugo kaolinite are shown in Fig. 4.

### Effect of H$_2$O$_2$ Concentration in the Presence of 10 M HNO$_3$ on Alumina Leaching

The results as depicted in Fig. 5 reveal that the fraction of alumina dissolved increases with increase in hydrogen peroxide concentration and leaching time. Dissolution rates of 48, 62, 70.9, 78.3, 85.6, and 85%, were recorded with hydrogen peroxide concentrations of 2, 4, 6, 8, 10, and 12 M, respectively, after leaching for 150 min. The result obtained with 12 M H$_2$O$_2$ (85.0 wt%) showed a slight decrease compared to that obtained with 10 M H$_2$O$_2$ (85.6 wt%) within a leaching time of 150 min, and this can be credited to the destruction of the clay structure at higher reagent concentration [14, 19]. Thus, 10 M H$_2$O$_2$ in 10 M HNO$_3$ was retained for further studies.

Figure 5 shows that about 85.6 wt% of alumina extraction was achieved in 150 min in 10 M hydrogen peroxide/10 M nitric acid binary solution. Hence, the leaching rate is higher when compared to using only HNO$_3$, where about 81.5 wt%
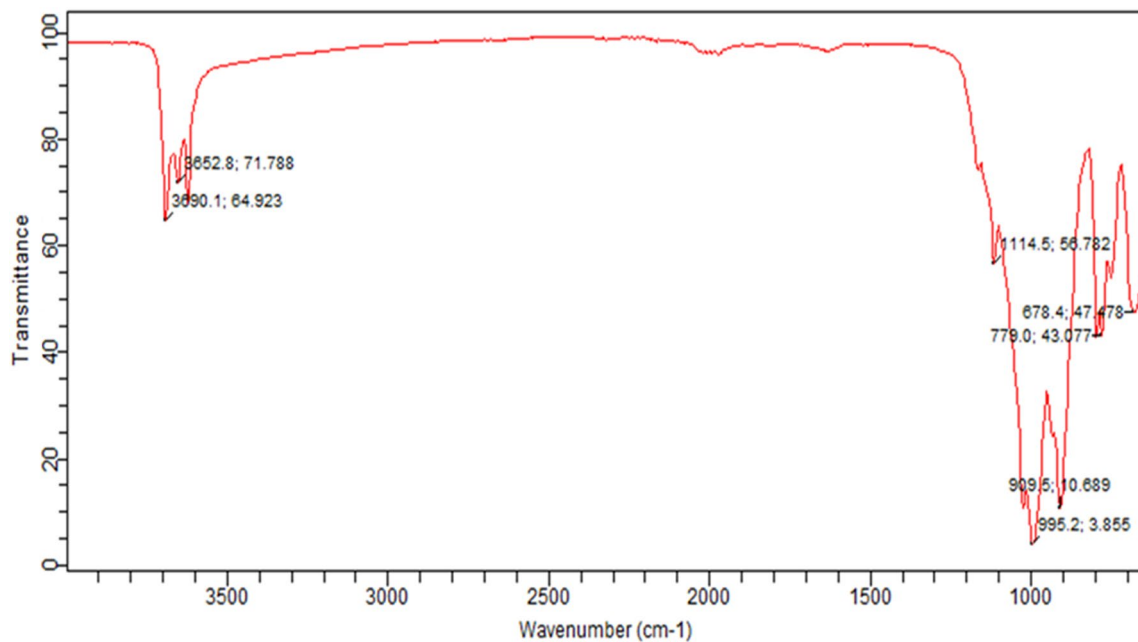
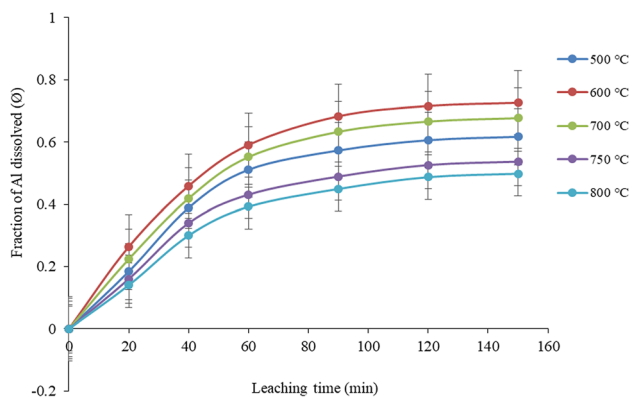**Fig. 3** FTIR spectra of Akpugo kaolinite



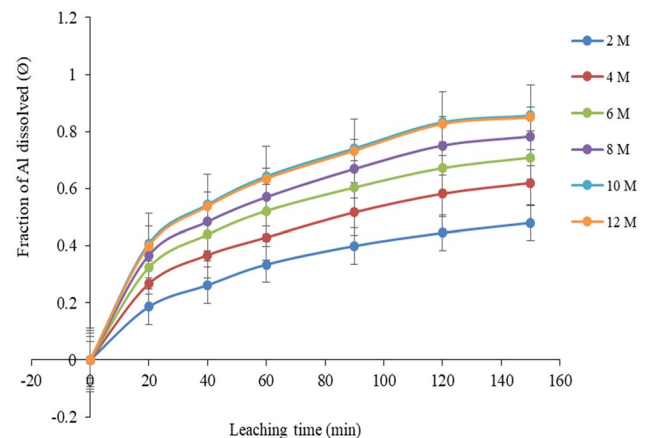**Fig. 4** Effect of calcinations temperature on alumina leaching



**Fig. 5** Effect of varied $H_2O_2$ concentration in the presence of 10 M $HNO_3$ on alumina leaching

was extracted at the same contact time [1]. This can be credited to the combined action of $O_2^{2-}$ and $NO_3^-$ ions in the solution.

## Effect of Stirring Rate on Alumina Leaching

The results on the influence of stirring rate on alumina dissolution in 10 M hydrogen peroxide/10 M nitric acid binary solution is depicted in Fig. 6. The results reveal that the percentage of alumina dissolved increases with increase in leaching time [20, 38, 39]. Alumina recovery rates of 49.8, 62.5, 75.9, 80.8, 86.8, and 87.3% were achieved after leaching for 150 min with stirring rates

of 90, 180, 360, 450, 540, and 720 rpm, respectively. Figure 6 reveals that the fraction of alumina dissolved depends on the stirring rate in the range of 90–540 rpm. As the stirring rate was increased above 540 rpm, stirring no longer had any noticeable influence on alumina recovery [14, 19].

A higher percentage (86.8%) was obtained with $H_2O_2$/ $HNO_3$ compared to 82.7% dissolution obtained with only $HNO_3$ at 540 rpm within a leaching time of 150 min. This could be credited to the combined action of $O_2^{2-}$ and $NO_3^-$ ions in the solution [40].
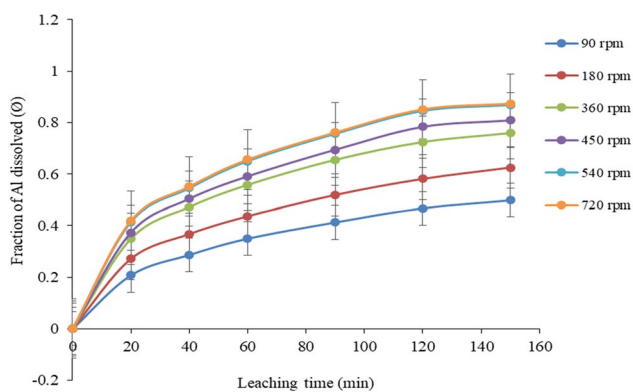
**Fig. 6** Effect of stirring rate on alumina leaching

## Effect of Temperature on Alumina Leaching

The results showing the influence of temperature on the rate of alumina recovery by 10 M hydrogen peroxide in the presence of 10 M nitric acid are depicted in Fig. 7. The result indicates that the percentage of alumina dissolved increased with increase in reaction temperature and leaching time [14, 19, 38]. Maximum dissolution rates of 47.6, 53.1, 71.6, 85.0, and 87.3% were obtained with leaching temperatures of 30, 40, 60, 80, and 90 °C, respectively, within 150 min. Hence, temperature positively affected Akpugo kaolinite dissolution rate. This may be credited to the fact that increase in temperature makes enough energy available for atomic and molecular collisions. Hence, the interaction between particles and the leachant increases the leaching rate. In addition, reaction constant, diffusivity and mass transfer coefficient, are enhanced by increase in temperature [39]. Equivalent results were recorded by Adekola et al. [10] in the dissolution kinetics of kaolin mineral in acidic media for predicting optimal condition for alum production and by Al-Zahrani and Abdul-Majid [41] on the extraction of alumina from local clays by hydrochloric acid process.
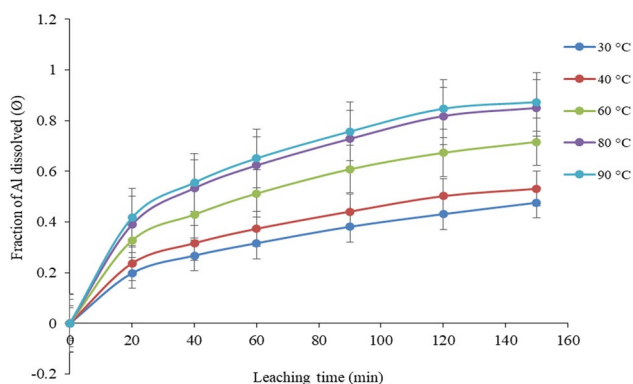
Interestingly, with a binary solution of 10 M hydrogen peroxide in 10 M nitric acid, about 87.3 wt% alumina dissolution was achieved within 150 min at 90 °C. The value obtained here is higher when compared to using only 10 M nitric acid as a leachant at the same conditions, and for which 83.6 wt% dissolution was obtained. Therefore, higher leaching rate achieved with 10 M $HNO_3$ in the presence of 10 M $H_2O_2$ could be credited to the combined action of $O_2^{2-}$ and $NO_3^-$ ions in the solution. Similar result was obtained by Nnanwube et al. [7].

## Effect of Solid/Liquid Ratio on Alumina Dissolution

The leaching curves are presented in Fig. 8, with the result showing an increase in the amount of alumina dissolved with decrease in S/L ratio. Dissolution rates of 86.6, 79.6, 66.9, 59.1, and 50.2% were achieved after 150 min of leaching with S/L ratios of 20, 25, 30, 35, and 45 g/L, respectively. Hence, increase in S/L ratio negatively influenced the leaching rate. This may be attributed to the increase in the amount of solid in the reaction mixture at a higher S/L ratio [24, 26, 42].

In the present study, about 86.6% of alumina dissolved within 150 min at 90 °C in 10 M $H_2O_2$ and 10 M $HNO_3$ binary solution. The results further reveal an increase in the percentage of the alumina dissolved when compared with 82.5% obtained when only $HNO_3$ was used [43]. This might be credited to the combined action of $O_2^{2-}$ and $NO_3^-$ ions in the solution.

## Effect of Particle Size on Alumina Leaching

The effect of particle size is depicted in Fig. 9 as a fraction of alumina recovered and reaction time. The fraction of alumina recovered was found to increase with decrease in particle size; hence, particle size negatively affected Akpugo kaolinite dissolution. Alumina recovery rates of 87.6, 80.5,
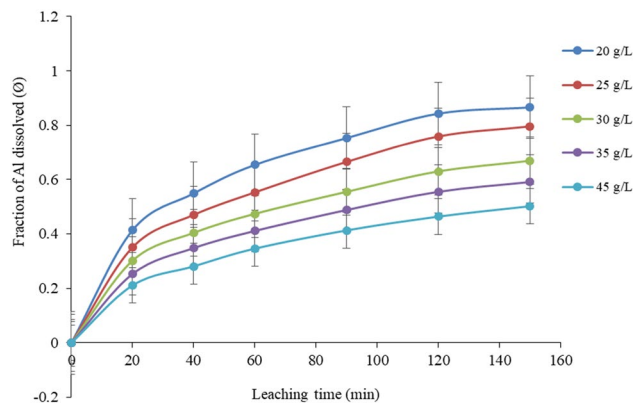


**Fig. 7** Effect of temperature on alumina leaching



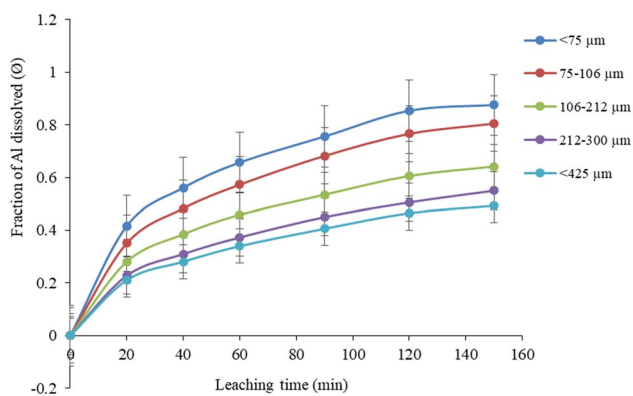**Fig. 8** Effect of solid/liquid ratio on alumina leaching

**Fig. 9** Effect of particle diameter on alumina leaching

64.2, 55, and 49.3% were achieved with particle diameters of < 75, 75–106, 106–212, 212–300, and < 425 µm, respectively. This is attributed to the fact that the particle-specific surface area varies inversely to its size. With smaller particle sizes and a larger specific area, more kaolinite is exposed to both $O_2^{2-}$ and $NO_3^-$ ions in the solution, which improves the kaolinite dissolution rate [40].

In this study, about 87.6% of alumina recovery was achieved within 150 min at 90 °C in 10 M hydrogen peroxide and 10 M nitric acid binary solution. The results further reveal an increase in the percentage of the alumina dissolved when compared with 83.5 wt% obtained when only $HNO_3$ was used within the same leaching time [1, 6, 7, 43]. This might be credited to the combined action of $O_2^{2-}$ and $NO_3^-$ ions in the solution.

## Dissolution Kinetics

A thorough understanding of the kinetics and mechanisms of heterogeneous fluid–solid reaction systems is important in the design of hydrometallurgical leaching processes. A number of studies have been carried out on these types of reactions, and many mathematical models have been developed [18]. Among the kinetic models that have been reported, they include the first- and second-order models [44], the shrinking core and the shrinking particle model [10, 45, 46], the mixed kinetic model [42], as well as the progressive conversion model [47].

A typical fluid–solid reaction is represented by Eq. (2):

$$aA(fluid) + bB(solid) \rightarrow Product, \tag{2}$$

where A and B represent the fluid used for the leaching reaction and the solid being leached, a and b represent the stoichiometric coefficient of the fluid and solid, respectively [48]. It has been reported that if the reaction rate in the bulk of solution was fast, the rate of ions from the solid's surface through the boundary layer would control the solution. Conversely, if the reaction rate is slow, it will control the overall process and the process will be controlled by chemical reaction; hence, boundary layer diffusion will not play any major role [49]. To establish the kinetics as well as the rate-controlling step of Akpugo kaolinite dissolution in nitric acid and hydrogen peroxide binary solution, the kinetic models in Table 4 were utilized [50]. The constants $k_3$-$k_8$ represent the rate constants for the various models, Ø denotes the conversion fraction of Akpugo kaolinite, while t denotes the leaching time [51].

Statistical and graphical methods were used to assess the fitness of the experimental data to the integrated rate equations. The experimental data on the effects of leachant concentration, temperature, S/L ratio, and particle size were fitted to each model in order to establish the kinetic model of the leaching process [52]. To achieve this, the graphs of each model were drawn against time [39]. From the model plots, the experimental data were found to fit into the product layer diffusion model for spherical particles [39]. This conformity indicates that Akpugo kaolinite exhibits high solubility in $HNO_3/H_2O_2$ binary solution. This is confirmed by the $R^2$ values of the fitted curves which are closest to unity for the product layer diffusion model as presented in Table 5 [38]. The rate constant values of the fitted models are also presented in Table 5.

**Table 4** Equations and mechanisms of dissolution of Akpugo kaolinite in a binary solution of nitric acid and hydrogen peroxide

| Equation | Mechanism | Eq. no |
|---|---|---|
| $k_3 t = 1 - (1-\text{Ø})^{\frac{1}{3}}$ | Surface chemical reaction (sp) | 3 |
| $k_4 t = 1 - 3(1-\text{Ø})^{\frac{2}{3}} + 2(1-\text{Ø})$ | Diffusion through the product layer (sp) | 4 |
| $k_5 t = 1 - (1-\text{Ø})^{\frac{1}{3}} + \frac{1}{6}[(1-\text{Ø})^{\frac{1}{3}} + 1 - 2(1-\text{Ø})^{\frac{2}{3}}]$ | Mixed control | 5 |
| $k_6 t = \text{Ø} + (1-\text{Ø})\text{In}(1-\text{Ø})$ | Diffusion through the product layer (cp) | 6 |
| $k_7 t = 1 - (1-\text{Ø})^{\frac{1}{2}}$ | Surface chemical reaction (cp) | 7 |
| $k_8 t = 1 - \frac{2}{3}\text{Ø} - (1-\text{Ø})^{\frac{2}{3}}$ | Solid film diffusion in remaining solid (sp) | 8 |

*sp* spherical particle, *cp* cylindrical particle

**Table 5** Rate constants and regression coefficients for Akpugo kaolinite dissolution in 10 M hydrogen peroxide/10 M nitric acid

| Concentration (M) | Apparent rate constant ($\times 10^{-3}$ min$^{-1}$) | | | | | | Correlation coefficient ($R^2$) | | | | | |
|---|---|---|---|---|---|---|---|---|---|---|---|---|
| | $K_3$ | $K_4$ | $K_5$ | $K_6$ | $K_7$ | $K_8$ | $k_3$ | $k_4$ | $k_5$ | $k_6$ | $k_7$ | $k_8$ |
| 2 | 1.53 | 0.689 | 2.21 | 0.972 | 2.20 | 0.230 | 0.817 | 0.996 | 0.798 | 0.994 | 0.793 | 0.994 |
| 4 | 2.15 | 1.280 | 3.06 | 1.760 | 3.03 | 0.429 | 0.810 | 0.997 | 0.780 | 0.994 | 0.774 | 0.997 |
| 6 | 2.65 | 1.860 | 3.72 | 2.500 | 3.67 | 0.620 | 0.787 | 0.992 | 0.750 | 0.985 | 0.742 | 0.991 |
| 8 | 3.11 | 2.460 | 4.31 | 3.230 | 4.24 | 0.820 | 0.825 | 0.994 | 0.785 | 0.987 | 0.772 | 0.994 |
| 10 | 3.71 | 3.290 | 5.05 | 4.180 | 4.94 | 1.100 | 0.846 | 0.990 | 0.800 | 0.983 | 0.784 | 0.991 |
| 12 | 3.65 | 3.210 | 4.98 | 4.090 | 4.87 | 1.070 | 0.848 | 0.990 | 0.804 | 0.984 | 0.790 | 0.990 |
| Stirring rate (rpm) | | | | | | | | | | | | |
| 90 | 1.61 | 0.759 | 2.33 | 1.070 | 2.31 | 0.250 | 0.789 | 0.995 | 0.765 | 0.993 | 0.763 | 0.996 |
| 180 | 2.17 | 1.300 | 3.07 | 1.790 | 3.05 | 0.433 | 0.806 | 0.998 | 0.775 | 0.995 | 0.772 | 0.998 |
| 360 | 2.97 | 2.280 | 4.12 | 2.990 | 4.06 | 0.753 | 0.809 | 0.996 | 0.771 | 0.985 | 0.759 | 0.993 |
| 450 | 3.31 | 2.730 | 4.56 | 3.540 | 4.47 | 0.909 | 0.839 | 0.991 | 0.799 | 0.986 | 0.786 | 0.992 |
| 540 | 3.82 | 3.440 | 5.18 | 4.360 | 5.06 | 1.150 | 0.858 | 0.991 | 0.813 | 0.984 | 0.798 | 0.990 |
| 720 | 3.87 | 3.520 | 5.25 | 4.440 | 5.12 | 1.170 | 0.857 | 0.990 | 0.813 | 0.983 | 0.798 | 0.989 |
| Temperature (°C) | | | | | | | | | | | | |
| 30 | 1.49 | 0.654 | 2.15 | 0.922 | 2.14 | 0.220 | 0.801 | 1.000 | 0.779 | 0.999 | 0.778 | 0.999 |
| 40 | 1.76 | 0.890 | 2.53 | 1.250 | 2.51 | 0.296 | 0.763 | 0.994 | 0.738 | 0.989 | 0.732 | 0.992 |
| 60 | 2.67 | 1.880 | 3.74 | 2.520 | 3.69 | 0.630 | 0.811 | 0.996 | 0.776 | 0.992 | 0.766 | 0.996 |
| 80 | 3.61 | 3.150 | 4.93 | 4.020 | 4.82 | 1.050 | 0.861 | 0.995 | 0.819 | 0.990 | 0.804 | 0.994 |
| 90 | 3.85 | 3.490 | 5.22 | 4.410 | 5.10 | 1.160 | 0.857 | 0.992 | 0.813 | 0.985 | 0.797 | 0.992 |
| Solid/liquid ratio (g/ml) | | | | | | | | | | | | |
| 20 | 3.81 | 3.420 | 5.17 | 4.330 | 5.05 | 1.140 | 0.850 | 0.990 | 0.805 | 0.982 | 0.789 | 0.990 |
| 25 | 3.14 | 2.510 | 4.34 | 3.280 | 4.37 | 0.837 | 0.874 | 0.995 | 0.839 | 0.995 | 0.866 | 0.995 |
| 30 | 2.40 | 1.560 | 3.39 | 2.120 | 3.35 | 0.520 | 0.798 | 0.996 | 0.767 | 0.992 | 0.757 | 0.996 |
| 35 | 2.02 | 1.140 | 2.87 | 1.570 | 2.84 | 0.380 | 0.800 | 0.997 | 0.775 | 0.994 | 0.766 | 0.997 |
| 45 | 1.62 | 0.760 | 2.33 | 1.070 | 2.31 | 0.255 | 0.795 | 0.998 | 0.776 | 0.996 | 0.770 | 0.997 |
| Particle size (μm) | | | | | | | | | | | | |
| <75 | 3.88 | 3.540 | 5.27 | 4.460 | 5.14 | 1.180 | 0.858 | 0.990 | 0.812 | 0.983 | 0.797 | 0.990 |
| 75–106 | 3.22 | 2.610 | 4.45 | 3.410 | 4.36 | 0.872 | 0.868 | 0.997 | 0.831 | 0.994 | 0.819 | 0.996 |
| 106–212 | 2.27 | 1.410 | 3.22 | 1.930 | 3.18 | 0.473 | 0.796 | 0.995 | 0.767 | 0.991 | 0.760 | 0.995 |
| 212–300 | 1.81 | 0.933 | 2.59 | 1.300 | 2.57 | 0.473 | 0.815 | 0.999 | 0.792 | 0.998 | 0.789 | 0.995 |
| <425 | 1.60 | 0.743 | 2.30 | 1.050 | 2.29 | 0.249 | 0.790 | 0.996 | 0.765 | 0.994 | 0.762 | 0.997 |

The reliance of the diffusion coefficient of the reaction on temperature can be used to estimate the apparent activation energy, $E_a$, according to the Arrhenius relation in Eq. (9) [53]:

$$k_d = A\exp\left(-\frac{E_a}{RT}\right), \tag{9}$$

where $k_d$ is the diffusion coefficient, $A$ denotes the pre-exponential factor, $E_a$ denotes the activation energy, $R$ denotes the ideal gas constant, and $T$ denotes temperature in Kelvin. Linearizing Eq. (9) gives Eq. (10). The values of $k_d$ were estimated from the slopes of the lines obtained by linearizing the curves in Fig. 7 as presented in Fig. 10. The activation energy, $E_a$, was estimated from the slope of the plot of In $k_d$ against $1/T$ as shown in Fig. 11 [24, 26, 54]. From Fig. 11,
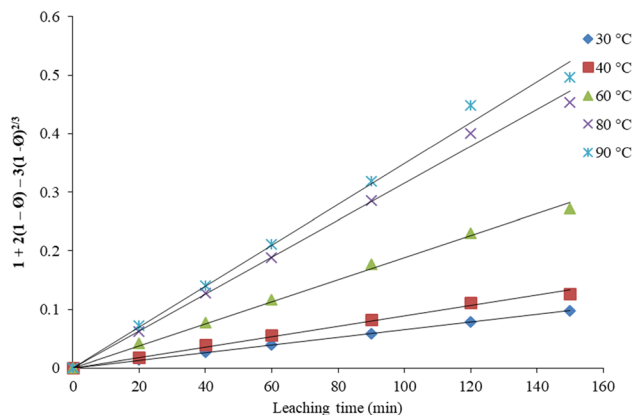


**Fig. 10** Plot of $1 + 2(1 - \varnothing) - 3(1 - \varnothing)^{2/3} = kt$ against leaching time at various temperatures
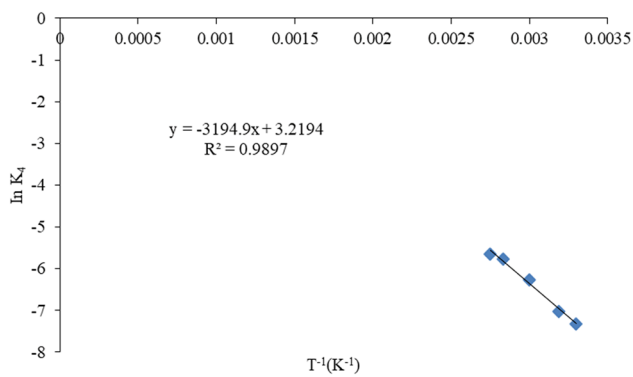
**Fig. 11** Arrhenius plot of reaction rate against reciprocal of temperature

activation energy was estimated to be 26,562.41 J/mol while the pre-exponential factor, A, was estimated to be 25.01 s$^{-1}$.

$$\ln k_d = \ln A - \frac{E_a}{RT}. \tag{10}$$

The activation energy obtained from this study falls within the range of the values reported in previous studies as presented in Table 6. Ajemba and Onukwuli [12] reported activation energy of 21.79 kJ/mol on the dissolution of Udi kaolinite in nitric acid solution in a process controlled by chemical reaction, while a value of 30.52 kJ/mol was reported for activation energy in another study (Ajemba and Onukwuli [13]) carried out on the dissolution of Ukpor kaolinite in nitric acid solution. On the other hand, Baba et al. [15] recorded activation energy value of 17.65 kJ/mol in their study on the treatment of Share kaolinite for improved industrial applications, in a process controlled by product layer diffusion. Adekola et al. [10] recorded activation energy of 21.60 kJ/mol in their study on the dissolution kinetics of Batagbon kaolin mineral in sulfuric and fluosilicic acid media for predicting optimal condition for alum production, in a process

controlled by mixed kinetics. In another study as reported in Table 6, Baba et al. [55] recorded activation energy value of 41.34 kJ/mol in their study on the bleaching of kaolin obtained from Egbeda in Osun state Nigeria, by oxalic acid leaching, in a process controlled by chemical reaction.

The mechanism of a leaching process may be predicted using the activation energy obtained from the reaction [56]. It has been reported that the activation energy of a process governed by diffusion is usually below 20 kJ/mol, while for a process controlled by chemical reaction, it has been reported to be above 40 kJ/mol [39]. However, it has been reported that in certain cases, the rate-determining step of a heterogeneous leaching process is preferably foretold from the graphs of kinetic equations instead of the activation energy [6, 19]. Hence, to obtain the rate-controlling step, the kinetic curves on the effect of parameters were linearized and plots of the rate constants obtained from the effect of particle sizes against the reciprocals of the particle radii as well as the reciprocal of the square of particle radii were made [14, 19, 20]. As postulated by the shrinking core model, the leaching kinetics is proportional to the reciprocal of the square of the original radius of the particle ($r_o$) for a process controlled by diffusion, while for a chemical reaction-controlled process, the kinetics varies with the reciprocal of the original radius of the particle [17, 57, 58]. From the plot of $k_d$ against ($1/r_o$) (Fig. 12), a linear relationship was obtained with $R^2$ value of 0.9959, while the plot of $k_d$ against ($1/r_o^2$) gave a correlation coefficient of 0.9601, indicating that the plot for chemical reaction mechanism gave a better fitting. Hence, the rate-controlling step in the leaching of Akpugo kaolinite in nitric acid and hydrogen peroxide binary solution is surface chemical reaction [45].

The influence of reaction parameters on the apparent rate constants can be established using the proposed empirical model depicted as Eq. (11):

$$k = k_o (LC)^e (d_p)^f \left(\frac{S}{L}\right)^g (w)^h e^{(-E_a/RT)}, \tag{11}$$

**Table 6** Estimated activation energy values from previous studies

| Clay type | Leachant | Activation energy ($E_a$) (kJ/mol) | Mechanism | Reference |
|-----------|----------|-----------|-----------|-----------|
| Kaolinite | Nitric acid | 21.79 | Chemical reaction | Ajemba and Onukwuli [12] |
| Kaolinite | Nitric acid | 30.52 | Product layer diffusion | Ajemba and Onukwuli [13] |
| Kaolinite | Hydrochloric acid and Hydrogen peroxide | 53.92 | Product layer diffusion | Nnanwube et al. [6] |
| Kaolinite | Oxalic acid | 17.65 | Product layer diffusion | Baba et al. [15] |
| Kaolinite | Sulfuric acid and Fluosilicic acid | 21.60 | Mixed control | Adekola et al. [10] |
| Kaolinite | Oxalic acid | 41.34 | Chemical reaction | Baba et al. [55] |
| Kaolinite | Nitric acid and hydrogen peroxide | 26.56 | Chemical Reaction | This study |
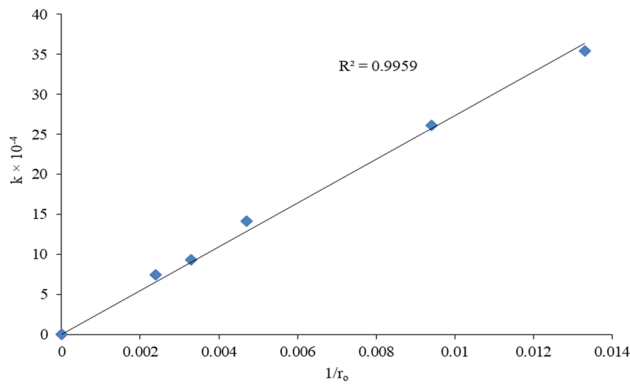
**Fig. 12** Plot of k against $1/r_o$



**Fig. 13** Plot of In $k_4$ against In (S/L)

where LC, $d_p$, S/L, w, $E_a$, R, T, and $k_o$ symbolize leachant concentration, particle size, solid/liquid ratio, stirring rate, activation energy, ideal gas constant, temperature, and frequency factor, respectively. The constants e, f, g, and h symbolize the reaction orders with respect to the respective reaction parameters [59]. Combining Eq. (4) and Eq. (11) gives Eq. (12).

$$1 - 3(1 - \varnothing)^{\frac{2}{3}} + 2(1 - \varnothing) = k_o(LC)^e \left(d_p\right)^f \left(\frac{S}{L}\right)^g (w)^h e^{(-E_a/RT)} t. \tag{12}$$

If other parameters are kept constant while only the concentration of the leachant is varied, Eq. (12) can be expressed as Eq. (13).

$$1 - 3(1 - \varnothing)^{\frac{2}{3}} + 2(1 - \varnothing) = k_o(LC)^e t. \tag{13}$$

Differentiation of Eq. (13) gives Eq. (14).

$$d[1 - 3(1 - \varnothing)^{\frac{2}{3}} + 2(1 - \varnothing)]/dt = k_o(LC)^e, \tag{14}$$

where d[1 + 2(1 − Ø) − 3(1 − Ø)$^{2/3}$]/dt represent the slope of the plot of 1 + 2(1 − Ø)−3(1 − Ø)$^{2/3}$ against time for various leachant concentrations shown in Fig. 5. Equation (14) is linearized by taking the logarithm of both sides of Eq. (14) [32]. A plot of In[d[1 + 2(1 − Ø) − 3(1 − Ø)$^{2/3}$]/dt] against In [LC] gives a slope equal to 'e' being the reaction order with respect to leachant concentration [60]. In a similar manner, the reaction orders with respect to stirring rate, solid/liquid ratio, and particle size were obtained by plotting In[d[1 + 2(1 − Ø) − 3(1 − Ø)$^{2/3}$]/dt] against In (w), In[d[1 + 2(1 − Ø) − 3(1 − Ø)$^{2/3}$]/dt] against In (S/L) (Fig. 13), and In[d[1 + 2(1 − Ø) − 3(1 − Ø)$^{2/3}$]/dt] against In ($d_p$) (Fig. 14), respectively.

The constants were estimated as follows: e = 0.907, f = −1.024, g = −1.928, and h = 0.781, respectively, for leachant concentration, particle size, solid/liquid ratio, and stirring rate. Therefore, putting the various estimated parameters into Eq. (12), at the optimum leaching conditions, together with the average alumina recovery rate
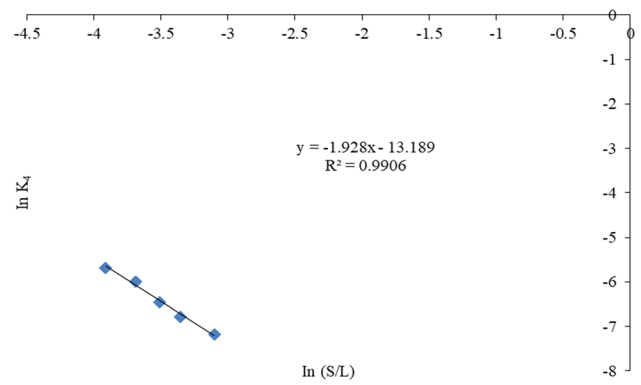
which was estimated to be 0.871, the overall rate constant, $k_o$, was estimated to be 8.883 s$^{-1}$. Hence, the kinetic expression that describes the leaching of Akpugo kaolinite in a binary solution of nitric acid and hydrogen peroxide is given as Eq. (15) [14].

$$1 - 3(1 - \varnothing)^{\frac{2}{3}} + 2(1 - \varnothing)$$
$$= 8.883(LC)^{0.907}(d_p)^{-1.024}\left(\frac{S}{L}\right)^{-1.928}(w)^{0.781} e^{\left(-\frac{26562.409}{RT}\right)} t. \tag{15}$$

Equation (15) is used to predict alumina leaching rate at the optimum conditions, and plots of the correlation between the experimental and predicted alumina recovery were made. The plots of the correlation between the experimental and predicted alumina recovery with respect to solid/liquid ratio and particle size are depicted in Figs. 15 and 16, respectively [43, 61].
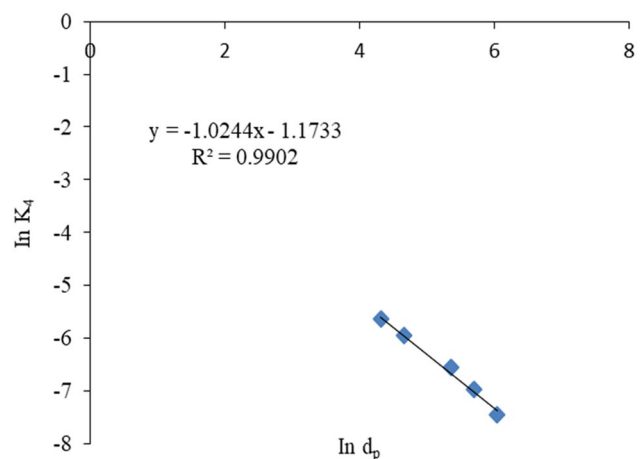

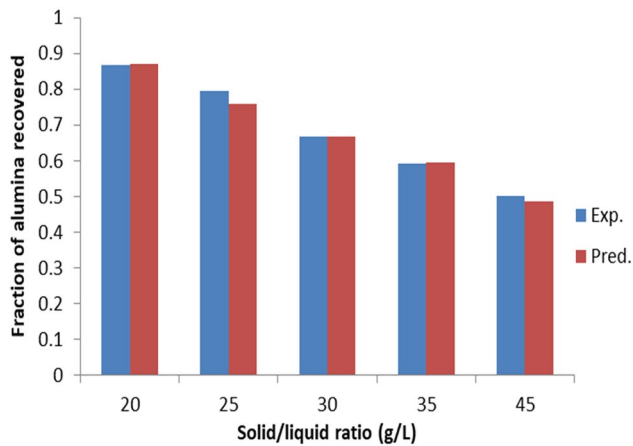
**Fig. 14** Plot of In $k_4$ against In $d_p$

**Fig. 15** Experimental versus predicted alumina recovery from the effect of solid/liquid ratio.
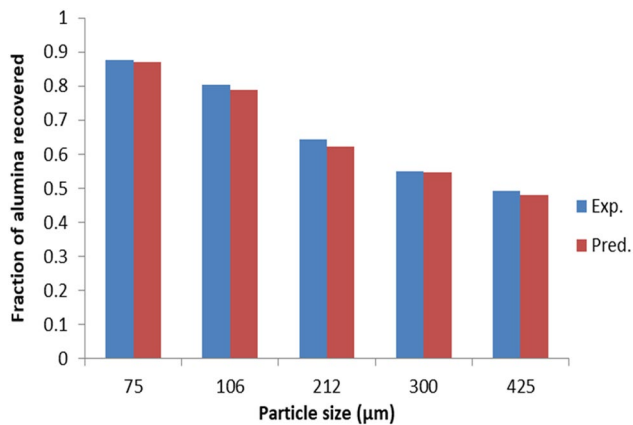


**Fig. 16** Experimental versus predicted alumina recovery from the effect of particle size

## Post-leaching Analysis

### SEM Analysis of Akpugo Kaolinite Leached with 10 M HNO₃/10 M H₂O₂

The results of the scanning electron microscope (SEM) of Akpugo kaolinite after leaching with 10 M HNO₃/10 M H₂O₂ binary solution are presented in Fig. 17 with magnifications of ×150 (a) and ×500 (b), respectively. The micrographs of the leaching residues show a progressive increase in the roughness of the solid. Similar observations were made by Souza et al. [60]. The particles have irregular shapes and form microscopic flakes with poor crystallinity [19, 20].

### XRD Analysis of Akpugo Kaolinite Leached with 10 M HNO₃/10 M H₂O₂

The analysis of Akpugo kaolinite after leaching with 10 M HNO₃/10 M H₂O₂ at 90 °C by XRD reveals the mineral phases found in the residue. The XRD analysis was carried out within a range of 5°–75° 2θ. The result revealed the major peaks at 19.73, 20.86, 26.65, 50.13, and 59.94 as shown in Fig. 18. The XRD data of the leached residue presented in Table 7 reveals the presence of Illite ($K_{4.00}Al_{16.00}Si_{8.00}O_{48.00}$) and Quartz ($Si_{3.00}O_{6.00}$) [14, 19, 23].

## Conclusions

The viability of nitric acid and hydrogen peroxide binary solution for alumina leaching from Akpugo kaolinite was investigated in this study. The mineral phases present in the clay were detected to be kaolinite and quartz via XRD analysis. Elemental analysis by XRF revealed the major oxides present in the clay as $Al_2O_3$, $SiO_3$, and $Fe_2O_3$. The minor oxides present in the clay were detected as MgO, $K_2O$, CaO, $Mn_2O_3$, and $TiO_2$, while $Cr_2O_3$, ZnO, and SrO were detected as traces. The fraction of alumina dissolved increases as the acid concentration, reaction temperature, and stirring rate increase and decrease as the S/L ratio and particle size increase. Six kinetic models were used to analyze the experimental data. The experimental data were found to fit into the product layer diffusion model while surface chemical reaction was the rate-controlling step. About 87.1% of the initial 20 g/L of alumina was recovered at the optimum conditions within 150 min. Activation energy was obtained to be 26.56 kJ/mol while the overall reaction constant was estimated to be 8.883 s⁻¹. Post-leaching residue analysis by XRD revealed the presence of illite and quartz. Hence, nitric acid and hydrogen peroxide binary solution proved to be a good leachant for alumina leaching.

**Fig. 17** SEM image of Akpugo kaolinite leached with 10 M $H_2O_2$ in 10 M nitric acid with magnifications of ×150 (**a**) and ×500 (**b**), respectively
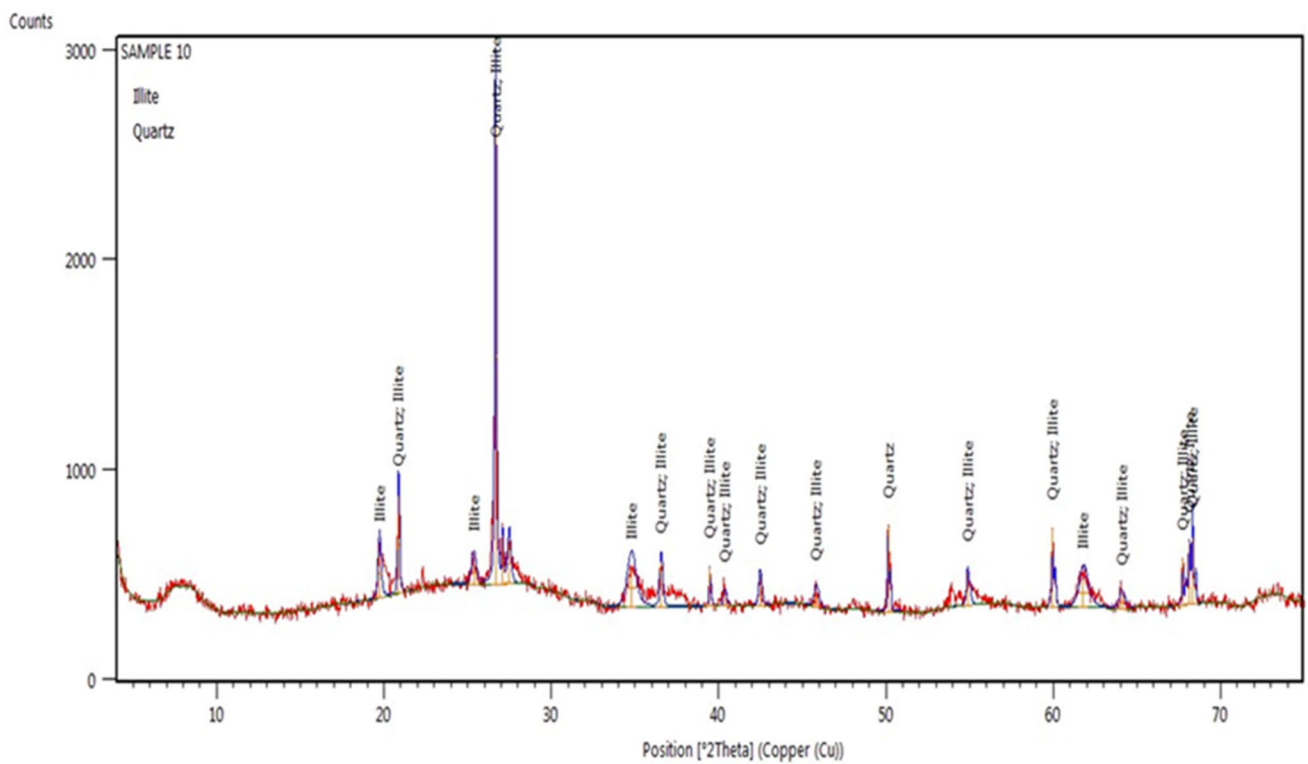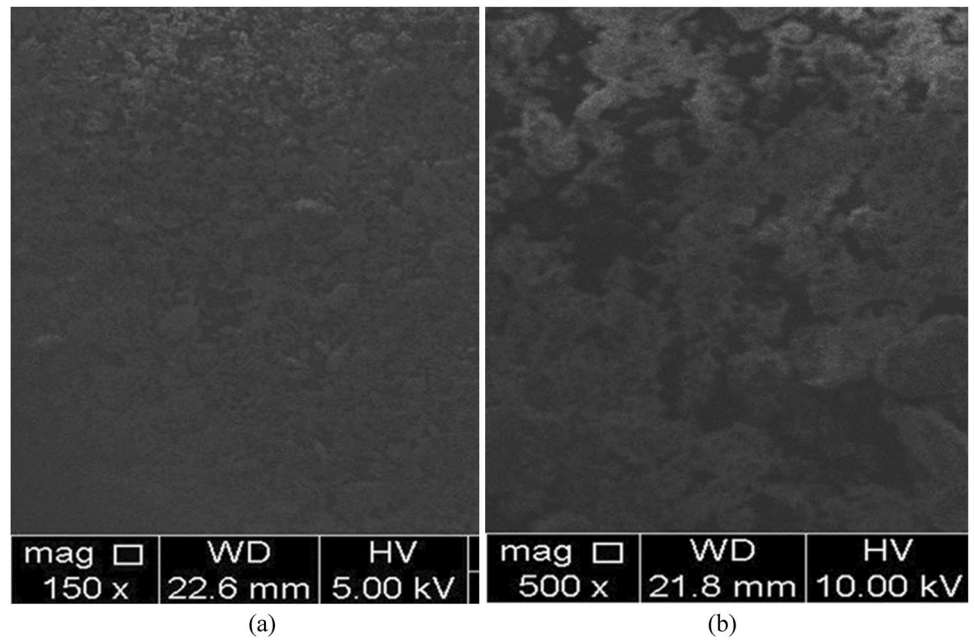


(a)  (b)



**Fig. 18** XRD pattern of the post-leached residue of Akpugo kaolinite clay after leaching for 150 min at 90 °C with 10 M $HNO_3$/10 M $H_2O_2$

**Table 7** The X-ray diffraction data of Akpugo kaolinite leached with 10 M HNO$_3$/10 M H$_2$O$_2$ showing the angle $2\theta$ and $d$-values of the compounds identified, with their relative intensity (%)

| $2\theta$ | $d$-value (Å) | Compound | Intensity (%) | JCPDS file No |
|---|---|---|---|---|
| 19.73 | 4.50 | Illite (K$_{4.00}$Al$_{16.00}$Si$_{8.00}$O$_{48.00}$) | 10.26 | 96-900-9666 |
| 20.86 | 4.26 | Quartz (Si$_{3.00}$O$_{6.00}$) Illite (K$_{4.00}$Al$_{16.00}$Si$_{8.00}$O$_{48.00}$) | 21.42 | 96-901-2601 96-900-9666 |
| 25.36 | 3.51 | Illite (K$_{4.00}$Al$_{16.00}$Si$_{8.00}$O$_{48.00}$) | 5.18 | 96-900-9666 |
| 26.65 | 3.35 | Quartz (Si$_{3.00}$O$_{6.00}$) Illite (K$_{4.00}$Al$_{16.00}$Si$_{8.00}$O$_{48.00}$) | 100.00 | 96-901-2601 96-900-9666 |
| 36.56 | 2.46 | Quartz (Si$_{3.00}$O$_{6.00}$) Illite (K$_{4.00}$Al$_{16.00}$Si$_{8.00}$O$_{48.00}$) | 9.94 | 96-901-2601 96-900-9666 |
| 50.13 | 1.82 | Quartz (Si$_{3.00}$O$_{6.00}$) | 18.47 | 96-901-2601 |
| 59.94 | 1.54 | Quartz (Si$_{3.00}$O$_{6.00}$) Illite (K$_{4.00}$Al$_{16.00}$Si$_{8.00}$O$_{48.00}$) | 17.24 | 96-901-2601 96-900-9666 |

JCPDS file No.: Joint Committee on Power Diffraction Standards File Number

## Declarations

## References

1. Nnanwube IA (2019) Kinetics and optimization studies on the hydrometallurgical recovery of zinc, lead, and alumina from their parent matrices, PhD Thesis, Nnamdi Azikiwe University

2. Keke M (2020) Kinetics and optimization of alumina recovery from Owhe clay, M. Eng. Thesis, Chukwuemeka Odumegwu Ojukwu University, Uli, Anambra State, Nigeria

3. Siddique NA, Kurny ASW (2010) Kinetics of leaching alumina from discarded high alumina refractory bricks. Int J Eng Technol 10(1):19–22

4. Liu Y, Naidu R (2014) Hidden values in bauxite residue (red mud): recovery of metals. Waste Manage 34:2662–2673. https://doi.org/10.1016/j.wasman.2014.09.003

5. Liu Y, Lin CX, Wu YG (2007) Characterization of red mud derived from a combined Bayer process and bauxite calcinations method. J Hazard Mater 146:255–261

6. Nnanwube IA, Keke M, Onukwuli OD (2022) Assessment of Owhe kaolinite as potential aluminium source in hydrochloric acid and hydrogen peroxide solutions: Kinetics modeling and optimization. Clean Chem Eng 2:100022

7. Nnanwube IA, Onukwuli OD, Ekumankama EO (2022) Assessment of Amagunze microcline for alumina recovery in nitric acid and hydrogen peroxide solutions and kinetic study. Can Metall Q. https://doi.org/10.1080/00084433.2022.2099725

8. Tantawy MA, Alomari AA (2019) Extraction of alumina from Nawan kaolin by acid leaching. Orient J Chem 35(3):1013–1021

9. Ibrahim KM, Moumani MK, Mohammad SK (2018) Extraction of γ-alumina from low-cost kaolin. MDPI 7(63):1–12. https://doi.org/10.3390/resources7040063

10. Adekola FA, Baba AA, Girigisu S (2017) Dissolution kinetics of kaolin mineral in acidic media for predicting optimal condition for alum production. J Central South Univ 23:318–324. https://doi.org/10.1007/s11771-017-3433-9

11. Pak VI, Kirov SS, Nalivaiko AY, Ozherelkov DY, Gromov AA (2019) Obtaining alumina from kaolin clay via aluminium chloride. MDPI 3938:1–12

12. Ajemba RO, Onukwuli OD (2012) Dissolution kinetics and mechanisms of reaction of Udi clay in nitric acid solution. Am J Sci Ind Res 3(3):115–121

13. Ajemba RO, Onukwuli OD (2012) Application of the shrinking core model to the analysis of alumina leaching from Ukpor clay using nitric acid. Int J Eng Res Technol 1(13):1–13

14. Nnanwube IA, Onukwuli OD (2018) Kinetics and mechanisms of nitric acid leaching of alumina from Amagunze clay. J Eng Appl Sci 13:63–82

15. Baba AA, Asala OO, Balogun AF, Kuranga IA, Bale RB, Adekola FA, Alabi AGF (2016) Treatment of a Nigerian kaolin ore for improved industrial application. Moroccan J Chem 4(1):119–127

16. Adebayo AO, Ipinmoroti KO, Ajayi OO (2006) Leaching of sphalerite with hydrogen peroxide and nitric acid solutions. J Miner Mater Charact Eng 5(2):167–177. https://doi.org/10.4236/jmmce.2006.52012

17. Aydogan S, Erdemoglu M, Ucar G, Aras A (2007) Kinetics of galena dissolution in nitric acid solutions with hydrogen peroxide. Hydrometallurgy 88:52–57

18. Baba AA, Olaoluwa DT, Alabi AGF, Balogun AF, Ibrahim AS, Sanni RO, Bale RB (2017) Dissolution behaviour of a beryl ore for optimal industrial beryllium compound production. Can Metall Q. https://doi.org/10.1080/00084433.2017.1403107

19. Nnanwube IA, Onukwuli OD (2018) Hydrometallurgical processing of a Nigerian galena ore in nitric acid: characterization and dissolution kinetics. J Miner Mater Charact Eng 6(3):271–293

20. Onukwuli OD, Nnanwube IA (2018) Hydrometallurgical processing of a Nigerian sphalerite ore in nitric acid: characterization and dissolution kinetics. Int J Sci Technol 6(3):40–54

21. Onukwuli OD, Okafor VN (2018) Thermodynamics and kinetics studies of alumina leaching from Karaworo clay using oxalic acid solutions. Int J Innov Eng Technol Sci 2(1):76–87

22. Nnanwube IA, Onukwuli OD (2020) Modeling and optimization of zinc recovery from Enyigba sphalerite in a binary solution of hydrochloric acid and hydrogen peroxide. J S Afr Inst Mining Metall 120(11):609–616

23. Nnanwube I, Onukwuli O (2020) Modeling and optimization of galena dissolution in a binary solution of nitric acid and ferric chloride using artificial neural network coupled with genetic algorithm and response surface methodology. S Afr J Chem Eng 32:68–77. https://doi.org/10.1016/j.sajce.2020.03.001

24. Nnanwube IA, Udeaja JN, Onukwuli OD (2020) Kinetics of zinc recovery from sphalerite in acetic acid solution. J Mater Environ Sci 11(3):499–511

25. Baba AA, Raji MA, Muhammed MO, Abdulkareem AY, Olasinde FT, Ayinda KI, Adekola FA, Bale RB (2019) Potential of a

Nigerian biotite-rich kaolinite ore to industrial alumina by hydrometallurgical process. Metall Res Technol 116(2):222. https://doi.org/10.1051/metal/2018076

26. Nnanwube I, Udeaja J, Onukwuli O (2020) Kinetics of zinc recovery from Enyigba Sphalerite in a binary solution of acetic acid and sodium nitrate. Aust J Basic Appl Sci 14(5):1–11

27. Okafor VN, Nnanwube IA, Obibuenyi JI, Onukwuli OD, Ajemba RO (2019) Removal of pigments from palm oil using activated Ibusa kaolinite: equilibrium, kinetic and thermodynamic studies. J Miner Mater Charact Eng 7:157–170

28. Okafor VN, Nnanwube IA, Onukwuli OD, Obibuenyi JI, Ajemba RO (2019) Modeling and process parameters optimization of colour pigments removal from palm oil using activated Ibusa clay. Int J Innov Stud Sci Eng Technol 5(7):26–32

29. Onukwuli OD, Okafor VN, Nnanwube IA, Obibuenyi JI, Ajemba RO (2019) Response surface optimization of pigments removal from palm oil using activated Karaworo clay. Int J Res Adv Eng Technol 5(3):36–41

30. Nnanwube IA, Onukwuli OD, Obibuenyi JI, Okafor VN, Ajemba RO (2020) Optimization of colour pigments removal from palm oil using activated Ogbunike kaolinite. Sigma J Eng Nat Sci 38(1):253–263

31. Nnanwube IA, Onukwuli OD, Okafor VN, Obibuenyi JI, Ajemba RO, Chukwuka CC (2020) Equilibrium, kinetics and optimization studies on the bleaching of palm oil using activated Karaworo kaolinite. J Mater Environ Sci 11(10):1599–1615

32. Baba AA, Adekola FA, Bale RB (2009) Study of dissolution kinetics of a Nigerian cassiterite ore by hydrochloric acid. Sci Focus 14(2):198–207

33. Bendou S, Amrani M (2014) Effect of hydrochloric acid on the structural of sodic-bentonite clay. J Miner Mater Charact Eng 2:404–413

34. Schroeder PA, Melear ND, Pruett RJ (2003) Quantitative analysis of anatine in Georgia kaolin using Raman spectroscopy. Appl Clay Sci 23:299–308

35. Divacaran R, Sivasankara VN (2004) Mechanism of kaolinite and titanium dioxide flocculation using chitosan-assistance by fulvic acids. Water Res 38:2135–2143

36. Raghavan P, Chandrasekhar S, Vogt V, Gock E (2004) Separation of titanoferrous impurities from kaolin by high shear pretreatment and froth flotation. Appl Clay Sci 25:111–120

37. Ohale PE, Uzoh CF, Onukwuli OD (2017) Optimal factor evaluation for the dissolution of alumina from Azaraegbelu clay in acid solution using RSM and ANN comparative analysis. S Afr J Chem Eng 24:43–54

38. Kocan F, Hicsonmez U (2019) Leaching of celestite in sodium hydroxide solutions and kinetic modeling. J Dispersion Sci Technol 40(1):43–54. https://doi.org/10.1080/01932691.2018.1464466

39. Kocan F, Hicsonmez U (2019) Leaching kinetics of celestite in nitric acid solutions. Int J Miner Metall Mater 26(1):11–20. https://doi.org/10.1007/s12613-019-1705-0

40. Ma J, Tang Y, Yang DQ, Pei P (2020) Kinetics of advanced oxidative leaching of pyrite in a potassium peroxydisulphate solution. J Southern Afr Inst Mining Metall 120:165–172

41. Al-Zahrani AA, Abdul-Majid MH (2009) Extraction of alumina from local clays by hydrochloric acid process. JKAU 20(2):29–41

42. Kunkul A, Gulezgin A, Demirkiran N (2013) Investigation of the use of ammonium acetate as an alternative lixiviant in the leaching of malachite ore. Chem Ind Chem Eng Quart 19(1):25–35. https://doi.org/10.2298/CICEQ120113033K

43. Baba AA, Adekola FA (2011) Comparative analysis of the dissolution kinetics of galena in binary solutions of HCl/FeCl$_3$ and HCl/H$_2$O$_2$. Int J Miner Metall Mater 18(1):1–9

44. Sobouti A, Hoseinian FS, Rezai B, Jalili S (2019) The lead recovery prediction from lead concentrate by an artificial neural network and particle swarm optimization. Geosyst Eng 22(6):319–327. https://doi.org/10.1080/12269328.2019.1644205

45. Osasona I, Oke OE, Adebayo AO (2021) Direct leaching of lead from galena using acetic acid in Iron (III) chloride. J Hazard Toxic Radioactive Waste 25(3):04021021. https://doi.org/10.1061/(ASCE)HZ.2153-5515.0000625

46. Baba AA, Kayode JO, Raji MA (2020) Low-energy feasibility for leaching an indigenous Scheelite ore for industrial applications. J Sustain Metall 6(4):659–666. https://doi.org/10.1007/s40831-020-00301-7

47. Baba AA, Adekola FA (2012) A study of dissolution kinetics of a Nigerian galena ore in hydrochloric acid. J of Saud Che Soc 16:377–386. https://doi.org/10.1016/j.jscs.2011.02.005

48. Wu DD, Wen SM, Yang J, Deng JS (2015) Investigation of dissolution kinetics of zinc from smithsonite in 5-sulphosalicylic acid solution. Can Metall Q 54(1):51–57. https://doi.org/10.1179/1879139514Y.0000000150

49. Awe SA, Samuelsson C, Sandstrom A (2010) Dissolution kinetics of tetrahedrite mineral in alkaline sulphide media. Hydrometallurgy 103(1–4):167–172. https://doi.org/10.1016/j.hydromet.2010.03.014

50. Adebayo AO, Adebayo MA, Olasehinde EF, Ojo OO (2021) Leaching kinetics of lead from galena using hydrogen peroxide and trichloroacetic acid. J Hazard Toxic Radioactive Waste 25(3):04021010. https://doi.org/10.1061/(ASCE)HZ.21535515.0000608

51. Yaras A, Arslanoglu H (2018) Leaching behavior of low-grade copper ore in the presence of organic acid. Can Metall Q 57(3):319–327. https://doi.org/10.1080/00084433.2018.1473136

52. Safarzadeh MS, Moradkhani D, Ojaghi-Ilkhchi M (2009) Kinetics of sulfuric acid leaching of Cadmium from Cd-Ni zinc plant residues. J Hazard Mater 163(2–3):880–890. https://doi.org/10.1016/j.jhazmat.2008.07.082

53. Wang S, Zheng K, Liu Q, Wang L, Feng X, Li H (2021) Galena weathering in simulated alkaline soil: lead transformation and environmental implications. Sci Total Environ 755(2):142708. https://doi.org/10.1016/j.scitotenv.2020.142708

54. Chen H, Gao P, Peng H, Wei H, Xie W, Wang H, Yang B (2019) Study on the hot deformation behavior and microstructure evolution of Cu-Cr-In alloy. J Mater Eng Perform 28:2128–2136. https://doi.org/10.1007/s11665-019-03961-z

55. Baba AA, Mosobalaje MA, Ibrahim AS, Girigisu S, Eletta OAA, Aluko FI, Adekola FA (2015) Bleaching of a Nigerian kaolin by oxalic acid leaching. J Chem Technol Metall 50(5):623–630

56. Ekmekyapar A, Demirkiran N, Kunkul A, Aktas E (2015) Leaching of malachite ore in Ammonium sulphate solutions and protection of copper oxide. Braz J Chem Eng 32(1):155–165. https://doi.org/10.1590/0104-6632.20150321s00003211

57. Aydogan S, Aras A, Canbazoglu M (2005) Dissolution kinetics of sphalerite in acidic ferric chloride leaching. Chem Eng J 144(1–3):67–72. https://doi.org/10.1016/j.cej.2005.09.005

58. Xue J, Zhong H, Wang S, Li C, Li J, Wu F (2016) Kinetics of reduction leaching of manganese dioxide ore with phytolacca Americana in sulfuric acid solution. J Saudi Chem Soc 20(4):437–442. https://doi.org/10.1016/j.jscs.2014.09.011

59. Dehghan R, Noaparast M, Kolahdoozan M (2009) Leaching and kinetic modelling of low-grade calcareous sphalerite in acidic ferric chloride solution. Hydrometallurgy 96(4):275–282. https://doi.org/10.1016/j.hydromet.2008.11.002

60. Souza AD, Pina PS, Leao VA (2007) Bioleaching and chemical leaching as an integrated process in the zinc industry. Miner Eng 20(6):591–599

61. Qu FS, Dong XF, Liu JY, Chen DM, Wang ZH, Zhou J (2018) The research on vacuum isothermal bloom for powder metallurgy V-5Cr-5Ti alloy guiding by the constitutive models and the error analysis. Int J Refract Metal Hard Mater 72:349–366. https://doi.org/10.1016/j.ijrmhm.2018.01.007

**Publisher's Note** Springer Nature remains neutral with regard to jurisdictional claims in published maps and institutional affiliations.